Relativistic Effects on Metal−Ligand Bond Strengths in π-Complexes: A Quasi-Relativistic Density Functional Study of $M(PH_3)_2X_2$ (M = Ni, Pd, Pt; $X_2 = O_2$, C_2H_2, C_2H_4) and $M(CO)_4(C_2H_4)$ (M = Fe, Ru, Os)

Jian Li, Georg Schreckenbach, and Tom Ziegler*

Department of Chemistry, University of Calgary, Calgary, Alberta, Canada T2N 1N4

Received August 3, 1994[⊗]

The strengths of the bonds between the d^{10} fragments $M(PH_3)_2$ (M = Ni, Pd, Pt) and the π-ligands O_2, C_2H_4, and C_2H_2, as well as the d^8 fragments $M(CO)_4$ (M = Fe, Ru, Os) and ethylene, have been studied by a density functional method based on the NL-SCF+QR scheme where nonlocal (NL) and quasi-relativistic (QR) corrections are included self-consistently. All calculations are based on fully optimized geometries of the complexes and fragments involved. The calculated bond energies display a V-like trend within a triad, with a minimum at the second-row transition metal complex. This trend is largely caused by relativistic effects which become very important for the 5d elements. Without relativity the bond strengths would decrease gradually down the triad. Relativistic effects destablize the d orbitals of the third-row transition metals and hence increase the metal to ligand back-donation as well as the bond strengths. Relativistic effects are also important for the geometries of the coordinated ligands O_2, C_2H_4, and C_2H_2. Thus, the O−O or C−C bond distances are stretched and the back-bending angles in C_2H_4 and C_2H_2 increased by relativistic effects in the 5d complexes.

Introduction

Complexes between metal fragments and unsaturated molecules such as N_2, O_2, CO, alkenes, and alkynes have been studied extensively.[1-3] The bonding between the metal center and the unsaturated ligands was first described by the Dewar−Chatt−Duncanson model.[4] In this model the occupied σ or π orbitals on the unsaturated molecules donate electron density to unoccupied metal d orbitals in synergy with a back-donation of electron density from the occupied d_π orbitals on the metal center to the empty π* orbital of the unsaturated ligands.

Much work has been carried out in order to understand how the relative degree of donation and back-donation is influenced by the ancillary ligands on the metal fragment, the nature of the unsaturated ligand, and the d-electron count on the metal center. We shall in the present study concentrate on how the synergy and bond strength change within a triad of transition metals. This work was prompted by recent studies[5] in which relativistic effects were shown to have a major effect on the M−CO and $M-CH_2$ bonds involving 5d elements.

We shall here explore the periodic trends within a triad of transition metals by investigating the d^{10} complexes $M(PH_3)_2X_2$ (M = Ni, Pd, Pt; $X_2 = O_2$, C_2H_4, C_2H_2) as well as the d^8 series $M(CO)_4(C_2H_4)$ (M = Fe, Ru, Os) by the most current density functional theory (DFT) techniques.[6] All energy calculations will be carried out on the basis of fully optimized geometries for both the complexes and the fragments. The impact of relativity on the bond strength in π-complexes will be examined in details by the aid of the extended transition state (ETS) method. It is the objective of our study to demonstrate that the relativistic enhancement of the bond strength is a common phenomenon in compounds where the metal−ligand bond can be described by the Dewar−Chatt−Duncanson bond model.

A previous DFT study of the π-bond strength in the d^{10} series $M(PH_3)_2X_2$ (M = Ni, Pd, Pt; X_2=O_2, C_2H_4, C_2H_2) was carried out by Ziegler[7] on the basis of the simple Hartree−Fock−Slater (HFS) method. In this investigation, experimental or assumed geometries were adopted and only Slater's Xα-type exchange functional was used in the energy calculations. Relativistic effects were only included to first order. A few *ab initio* studies have also been carried out on some of the title systems by Sakaki *et al.*[8] However, the issue of periodic trends was not addressed in these investigations.

Computational Details

All calculations in this study were carried out by using the density functional package, ADF, developed by Baerends *et al.*[9] and vectorized by Ravenek.[10] The adopted numerical integration scheme was that developed by te Velde *et al.*[11] A set of uncontracted triple-ζ Slater-type orbitals (STO) was employed for the *n*s, *n*p, *n*d, (*n*+1)s, and

[⊗] Abstract published in *Advance ACS Abstracts,* May 15, 1995.

(1) (a) Chatt, J.; Dilworth, J. R.; Richards, R. L. *Chem. Rev.* **1978**, *78*, 589. (b) Vaska, L. *Acc. Chem. Res.* **1976**, *9*, 175. (c) Lukehart, C. M. *Fundamental Transition Metal Organometallic Chemistry*; Brooks/Cole: Monterey, CA, 1985. (d) Hartley, F. R. In *Comprehensive Organometallic Chemistry*; Wilkinson, G., Ed.; Pergamon: Oxford, U.K., 1982; Vol. 6.

(2) (a) Chatt, J.; da Camara Piaa, C. L. M.; Richards, R. L. *New Trends in the Chemistry of Nitrogen Fixation*; Academic Press: London, 1980. (b) Anderson, J. R.; Boudart, M. *Catalysis, Science and Technology*; Springer-Verlag: Heidelberg, Germany, 1984. (c) Moser, W. R.; Slocum, D. W. *Homogeneous Transition Metal Catalyzed Reactions*; Advances in Chemistry Series 230; American Chemical Society: Washington, DC, 1992.

(3) (a) Klotz, I. M.; Kurtz, D. M., Jr. Metal−Dioxygen Complexes. *Chem. Rev. (Thematic Issue)* **1993**, *94* (3). (b) Boca, R. *Coord. Chem. Rev.* **1983**, *50*, 1.

(4) (a) Dewar, M. J. S. *Bull. Soc. Chim. Fr.* **1951**, *18*, C79. (b) Chatt, J.; Duncanson, L. A. *J. Chem. Soc.* **1953**, 2339.

(5) (a) Li, J.; Schreckenbach, G.; Ziegler, T. *J. Phys. Chem.* **1994**, *98*, 4838. (b) Li, J.; Schreckenbach, G.; Ziegler, T. *J. Am. Chem. Soc.* **1995**, *117*, 486. (c) Jacobsen, H.; Schreckenbach, G.; Ziegler, T. *J. Phys. Chem.* **1994**, *98*, 11410.

(6) (a) Parr, R. G.; Yang, W. *Density Functional Theory of Atoms and Molecules*; Oxford University Press: New York, 1988. (b) Labanowski, J.; Andzelm, J. *Density Functional Methods in Chemistry*; Springer- Verlag: Heidelberg, Germany, 1991. (c) Ziegler, T. *Chem. Rev.* **1991**, *91*, 651.

(7) Ziegler, T. *Inorg. Chem.* **1985**, *24*, 1547.

(8) (a) Kitaura, K.; Sakaki, S.; Morokuma, K. *Inorg. Chem.* **1981**, *20*, 2292. (b) Sakaki, S.; Ohkubo, K. *J. Phys. Chem.* **1989**, *93*, 5655. (c) Sakaki, S.; Ieki, M. *Inorg. Chem.* **1991**, *30*, 4218. (d) Sakaki, S.; Ogawa, M.; Musashi, Y.; Arai, T. *Inorg. Chem.* **1994**, *33*, 1660.

(9) Baerends, E. J.; Ellis, D. E.; Ros, P. *Chem. Phys.* **1973**, *2*, 41.

0020-1669/95/1334-3245$09.00/0

$(n+1)$p valence orbitals of the transition metal atoms.[12] For the 2s and 2p orbitals of carbon and oxygen, use was made of a double-ζ basis augmented by an extra 3d polarization function. The inner core shells were treated by the frozen-core approximation. A set of auxiliary s, p, d, f and g STO functions, centered on all nuclei, was introduced to fit the molecular density and to present Coulomb and exchange potentials accurately.[13] All molecular geometries were optimized according to the analytic energy gradient method implemented by Verslius and Ziegler[14] at the LDA level[15] and by Fan and Ziegler[16] at the nonlocal (NL) level, NL-SCF. The NL corrections adopted were based on Becke's[17] functional for exchange and Perdew's[18] functional for correlation.

The relativistic effects were taken into account by retaining terms up to first order in α^2 (α is the fine structure constant) in the Hamiltonian

$$\mathbf{H} = \mathbf{H}^0 + \alpha^2\mathbf{H}^1 \qquad (1)$$

where $\mathbf{H}^1$ includes contributions from the mass-velocity, Darwin, and spin−orbit terms

$$\mathbf{H}^1 = \mathbf{H}_{mv} + \mathbf{H}_{Darw} + \mathbf{H}_{SO} \qquad (2)$$

In the lower level scheme based on first-order perturbation theory (FO),[19] the relativistic contribution to the total energy is calculated as

$$E^1 = \langle \Psi^0 | \mathbf{H}_{mv} + \mathbf{H}_{Darw} + \mathbf{H}_{SO} | \Psi^0 \rangle \qquad (3)$$

where ψ^0 is the nonrelativistic wave function.

In the more elaborate quasi-relativistic method (QR)[20] changes in the density induced by the first-order Hamiltonian (2) are taken into account to all orders of α^2 whereas operators in the Hamiltinian to second and higher orders are neglected. The QR scheme can readily be extended to include energy gradients of importance for structure optimizations.[21]

Results and Discussion

We shall in the first three sections discuss the impact of relativity on the structure and stability of the title compounds by simply presenting the calculated results and correlate them with experimental data and geometries derived from *ab initio* calculations. A rationale for the relativistic effects will be given in section 4.

1. Dioxygen Complexes $M(PH_3)_2O_2$ (M = Ni, Pd, Pt). Dioxygen can coordinate both end-on and side-on to a metal center.[22,23] Here we only consider the case in which O_2 coordinates side-on to the d^{10} $M(PH_3)_2$ (M = Ni, Pd, Pt) fragments. The electronic structures of the fragments and the adduct have been analyzed in detail elsewhere.[7] Due to steric factors, the $M(PH_3)_2$ fragments are linear in the free state, **1**, while both steric and electronic factors favor a bent conformation in the adducts, **2**.

Table 1. Optimized Geometries of $M(PH_3)_2$ and $M(PH_3)_2O_2$[a]

molecule	method	O−O	M−O	M−P	∠PMP
	Calculated				
$Ni(PH_3)_2$	NL-SCF+QR			2.130	180.0
$Pd(PH_3)_2$	NL-SCF+QR			2.274	180.0
	HF[b]			2.408	180.0
	MP2[b]			2.34	180.0
$Pt(PH_3)_2$	NL-SCF+QR			2.302	180.0
	HF[c]			2.333	180.0
	HF[d]			2.298	180.0
O_2	NL-SCF+QR	1.233			
$Ni(PH_3)_2O_2$	NL-SCF	1.440	1.837	2.144	108.0
	NL-SCF+QR	1.442	1.832	2.140	107.0
$Pd(PH3)_2O_2$	NL-SCF	1.392	2.066	2.365	107.2
	NL-SCF+QR	1.420	2.029	2.293	113.2
$Pt(PH3)_2O_2$	NL-SCF	1.390	2.145	2.440	104.6
	NL-SCF+QR	1.454	2.032	2.329	96.0
	Experimental				
$Pd[PPh(Bu^t)_2]_2$[e]				2.285	
$Pt[PPh(Bu^t)_2]_2$[e]				2.252	
O_2[f]		1.207			
$Ni(CNBu^t)_2O_2$[g]		1.45	1.808		
$Pd[PPh(Bu^t)_2]_2O_2$[h]		1.37	2.06	2.358	115
$Pt[PPh(Bu^t)_2]_2O_2$[h]		1.43	2.02	2.29	113

[a] Bond lengths in angstroms and bond angles in degrees. [b] Reference 8a. [c] Reference 8c. [d] Reference 25. [e] Reference 24. [f] Reference 26. [g] Reference 27. [h] Reference 28.

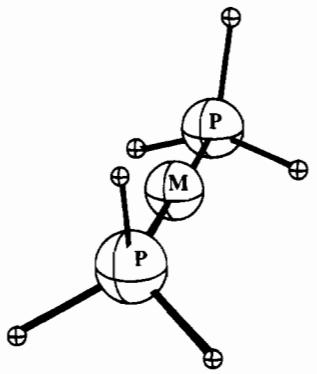

1

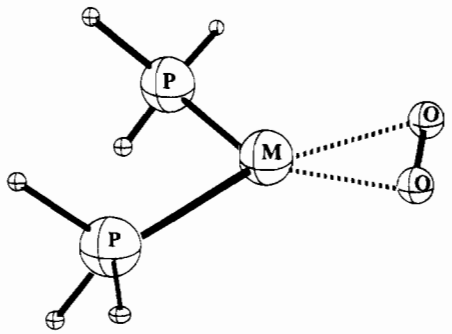

2

The optimized geometries for $M(PH_3)_2$ in the free linear state, **1**, are given in Table 1. A few experimental geometries[24] are available for comparison. Experimental structures[24] have the Pd−P and Pt−P distances in the range 2.26−2.33 Å, well within the limits calculated by the NL-SCF+QR method. Sakaki *et al.*[8a] partially optimized the Pd−P distance of $Pd(PH_3)_2$ with

(10) Ravenek, W. In *Algorithms and Applications on Vector and Parallel Computers;* te Riele, H. J. J., Dekkar, Th. J., van de Vorst , H. A., Eds.; Elsevier: Amsterdam, 1987.
(11) (a) Boerrigter, P. M.; te Velde, G.; Baerends, E. J. *Int. J. Quantum Chem.* **1988**, 33, 87. (b) te Velde, G.; Baerends, E. J. *J. Comput. Phys.* **1992**, *99*, 84.
(12) (a) Snijders, J. G.; Baerends, E. J.; Vernooijs, P. *At. Nucl. Data Tables* **1982**, *26*, 483. (b) Vernooijs, P.; Snijders, J. G.; Baerends, E. J. Slater type basis functions for the whole periodic system. Internal report, Free University of Amsterdam, The Netherlands, 1981.
(13) Krijn, J.; Baerends, E. J. Fit functions in the HFS-method. Internal report (in Dutch), University of Amsterdam, The Netherlands, 1984.
(14) Versluis, L.; Ziegler, T. *J. Chem. Phys.* **1988**, *88*, 322.
(15) Vosko, S. H.; Wilk, L.; Nusair, M. *Can. J. Phys.* **1980**, *58*, 1200.
(16) Fan, L.; Ziegler, T. *J. Chem. Phys.* **1991**, *95*, 7401.
(17) Becke, A. *J. Chem. Phys.* **1986**, *84*, 4524.
(18) Perdew, J. P. *Phys. Rev. B* **1986**, *33*, 8822. Erratum. *Ibid.* **1986**, *34*, 7406.
(19) (a) Snijders, J. G.; Baerends, E. J. *Mol. Phys.* **1978**, *36*, 1789. (b) Snijders, J. G.; Baerends, E. J.; Ros, P. *Mol. Phys.* **1979**, *38*, 1909.
(20) Ziegler, T.; Tschinke, V.; Baerends, E. J.; Snijders, J. G.; Ravenek, W. *J. Phys. Chem.* **1989**, *93*, 3050.
(21) Schreckenbach, G.; Ziegler, T.; Li, J. *Int. J. Quantum Chem.*, in press.
(22) Gubelmann, M. H.; Williams, A. F. *Struct. Bonding* **1983**, *55*, 1.
(23) Bytheway, I.; Hall, M. B. *Chem. Rev.* **1994**, *94*, 639.
(24) Otsuka, S.; Yoshida, T.; Matsumoto, M.; Nakatsu, K. *J. Am. Chem. Soc.* **1976**, *98*, 5850.

the Hartree−Fock (HF) scheme as well as the second-order Møller−Plesset (MP2) method. The MP2 Pd−P length is significantly shorter than that determined by the HF scheme but still about 0.07 Å longer than our NL-SCF+QR estimate. The deviation is most likely due to the small basis set used in the HF and MP2 calculations. In a careful study of the role played by d orbitals on phosphorus atoms, Fantucci[25] optimized the geometry of $Pt(PH_3)_2$ at the HF level. The Pt−P distance obtained in this study compares fairly well with our NL-SCF+QR estimate. The *ab initio* calculations included relativistic effects by making use of effective core potentials.

The optimized geometries for the adducts, **2**, $M(PH_3)_2O_2$ (M = Ni, Pd, Pt) are shown in Table 1 together with experimental geometries for some analogous compounds determined by X-ray crystallography.[26−28] Our calculated geometries, especially with regard to the MO_2 framework, compare well with the experimental results. The experimental M−P distances and P−M−P angles refer to bulky phosphines. Thus, a direct comparison to our PH_3 model systems is not possible. However, the M−P values calculated by the NL-SCF+QR method are certainly in the range observed experimentally.

The optimized structures display a significant elongation of the O−O distance upon coordination relative to free O_2 with R = 1.21 Å, Table 1. The O−O distances are 1.442, 1.420, and 1.454 Å at the NL-SCF+QR level for the Ni, Pd, and Pt complexes, respectively, compared to 1.45, 1.37, and 1.43 Å in the corresponding experimental geometries. By summarizing the known experimental data, Vaska [1b] pointed out that the O−O distance in side-on complexes is close to the values of 1.48 Å found in H_2O_2 and O_2^{2-}. Our calculated O−O bond lengths are in accordance with this observation. Relativistic effects are seen to contract the M−O and M−P bond distances by as much as 0.06 Å for the 4d element and up to 0.12 Å for the 5d element. The relativistic O−O bond increase is 0.06 Å for platinum, and we note that the O−O distance in the 4d complex, in agreement with experiment, becomes the shortest after the inclusion of relativity (NL-SCF+QR). To our knowledge, there is no systematic *ab initio* study on the dioxygen complexes of the Pd triad.

The M−O_2 bond energy, ΔE, between $M(PH_3)_2$ and O_2 in $M(PH_3)_2O_2$ corresponds to the negative of the formation energy in the process

$$M(PH_3)_2 + O_2 \rightarrow M(PH_3)_2O_2 \qquad (4)$$

Thus, ΔE is calculated according to

$$\Delta E = E[M(PH_3)_2] + E[O_2] - E[M(PH_3)_2O_2] \qquad (5)$$

where $E[M(PH_3)_2O_2]$ and $E[M(PH_3)_2]$ are the energies of $M(PH_3)_2O_2$, **2**, and $M(PH_3)_2$, **1**, respectively, whereas $E[O_2]$ is the energy of O_2 in its triplet $^3\Sigma_g$ ground state. Since the zero-point energy correction is excluded, ΔE represents only the electronic contribution to the bond enthalpy. The calculated ΔE values for $M(PH_3)_2O_2$ with M = Ni, Pd, Pt are shown in Table 2. We shall first concentrate on the highest level of nonrelativistic DFT theory, NL-SCF, as well as its relativistic extension, NL-SCF+QR.

At the NL-SCF+QR level, ΔE is 45.1, 15.5, and 21.1 kcal/mol for the Ni, Pd, and Pt complexes, respectively. Relativity enhances the $(PH_3)_2Pt-O_2$ bond strength by 14 kcal/mol. As a result, the $(PH_3)_2Pd-O_2$ bond becomes the weakest in the triad. There are no experimental data or *ab initio* studies available for a direct comparison. The enthalpies of association for the addition of O_2 to $Rh(cis\text{-}Ph_2PCH{=}CHPPh_2)_2^{+}$ [29] and *trans*-$[IrCl(CO)PPh_3)_2]$[30] were determined to be −11 and −17 kcal/mol, respectively. Our calculated ΔE's at the NL-SCF+QR level for the corresponding 5d element platinum are in line with these estimates. The calculated trend for ΔE within the triad is also in agreement with qualitative observations. Thus experimental equilibrium constants for O_2 association point to the stability order 3d > 5d > 4d.[31]

Table 2. DFT-Calculated M−X_2 Bond Energies[b] for $M(PH_3)_2X_2$ (X_2 = O_2, C_2H_4, C_2H_2) and $Os(CO)_4(C_2H_4)$[a]

	LDA	LDA/NL	LDA/NL+FO	NL-SCF	NL-SCF+FO	NL-SCF+QR
$Ni(PH_3)_2O_2$	59.8	43.6	44.6	44.3	45.4	45.1
$Pd(PH_3)_2O_2$	23.3	9.2	14.2	10.4	14.1	15.5
$Pt(PH_3)_2O_2$	22.8	7.3	20.6	7.2	15.9	21.1
$Ni(PH_3)_2(C_2H_4)$	52.3	34.1	35.8	36.5	38.4	38.0
$Pd(PH_3)_2(C_2H_4)$	32.4	15.1	19.1	15.9	17.5	19.8
$Pt(PH_3)_2(C_2H_4)$	29.4	12.2	22.0	13.5	16.3	22.8
$Ni(PH_3)_2(C_2H_2)$	59.4	41.4	43.9	43.4	45.7	45.3
$Pd(PH_3)_2(C_2H_2)$	32.9	16.3	21.3	16.5	19.7	21.8
$Pt(PH_3)_2(C_2H_2)$	28.2	11.8	25.7	12.4	17.6	24.8
$Fe(CO)_4(C_2H_4)$	56.3	36.3	37.3	38.0	39.2	38.9
$Ru(CO)_4(C_2H_4)$	42.0	24.1	27.6	23.0	26.6	30.7
$Os(CO)_4(C_2H_4)$	46.1	25.9	39.6	27.4	38.4	39.3

[a] LDA/NL means that the geometry is optimized at the LDA level and the nonlocal (NL) corrections are treated as perturbations. In LDA/NL+FO, relativistic effects are included as a first-order (FO) perturbation. For NL-SCF+FO, the nonlocal corrections are treated self-consistently whereas the relativistic corrections are added still as a first-order perturbation. For NL-SCF+QR both nonlocal and relativistic corrections are included self-consistently. [b] All energies are in kcal/mol.

Also shown in Table 2 are bond energies calculated at levels of theory other than NL-SCF and NL-SCF+QR. The simple LDA scheme affords much larger bond energies than the nonlocal NL-SCF method. It is a general experience that LDA overestimates the strengths of bonds.[6b,c] In Table 2 all LDA values correspond to geometries optimized at the LDA level. Calculating the nonlocal bond energies at the LDA geometries, LDA/NL, affords estimates in good agreement with results from the fully self-consistent NL-SCF scheme. This is encouraging since the NL-SCF method is 3−4 times more demanding than the LDA/NL scheme. We have also evaluated relativistic effects to first order (FO) and added the contributions to the LDA/NL results, LDA/NL+FO, as well as the NL-SCF estimates, NL-SCF+FO. These bond energies should be compared to the fully self-consistent NL-SCF+QR data. It is encouraging to note that the computationally much more expedient (4−6 times) LDA/NL+FO scheme affords bond energies in good agreement with the NL-SCF+QR values. We shall in the following base our discussion exclusively on the highest level of nonrelativistic, NL-SCF, and relativistic, NL-SCF+QR, theory, respectively.

2. Ethylene and Acetylene Complexes $M(PH_3)_2(C_2H_4)$ and $M(PH_3)_2(C_2H_2)$ (M = Ni, Pd, Pt). Ethylene and acetylene adducts are among the most extensively studied organometallic π-complexes. In fact, the Dewar−Chatt−Duncanson model was first proposed in connection with studies of Zeise's platinum ethylene complex $K[PtCl_3(C_2H_4)]$.[4b] We shall in this section

(25) Fantucci, P. *Comments Inorg. Chem.* **1992**, *13*, 241.
(26) Abrahams, J. C. *Q. Rev. Chem. Soc.* **1956**, *10*, 407.
(27) Matsumoto, M.; Nakatsu, K. *Acta Crystallogr., B* **1975**, *31*, 2711.
(28) Yoshida, T.; Tatsumi, K.; Matsumoto, M.; Nakatsu, K.; Nakamura, A.; Fueno, T.; Otsuka, S. *Nouv. J. Chem.* **1979**, *3*, 761.
(29) Vaska, L.; Patel, R. C.; Brady, R. *Inorg. Chim. Acta* **1978**, *30*, 239.
(30) Vaska, L. *Acc. Chem. Res.* **1968**, *1*, 335.
(31) (a) Mondal, J. U.; Blake, D. M. *Coord. Chem. Rev.* **1982**, *47*, 205. (b) Mondal, J. U.; Bulls, A. R.; Blake, D. M. *Inorg. Chem.* **1982**, *21*, 1668.

Table 3. Optimized Geometries of $M(PH_3)_2(C_2H_4)$ and $M(PH_3)_2(C_2H_2)$[a]

molecule	method	C−C	M−C	∠PMP	θ[n]
	Calculated				
C_2H_4	NL-SCF+QR	1.337			
$Ni(PH_3)_2(C_2H_4)$	NL-SCF	1.412	1.983	109.9	24.0
	NL-SCF+QR	1.414	1.981	109.0	24.3
	HF[b,c]	1.42	1.95	(120)	26
$Pd(PH_3)_2(C_2H_4)$	NL-SCF	1.384	2.220	117.1	18.1
	NL-SCF+QR	1.407	2.182	110.8	19.5
$Pt(PH_3)_2(C_2H_4)$	NL-SCF	1.387	2.284	110.6	16.3
	NL-SCF+QR	1.422	2.180	104.9	21.4
	HF[d]	1.411	2.174	107	22
C_2H_2	NL-SCF+QR	1.205			
$Ni(PH_3)_2(C_2H_2)$	NL-SCF	1.280	1.902	106.9	31.5
	NL-SCF+QR	1.282	1.900	106.4	31.6
	HF[b]	1.28	1.89	(120)	40
$Pd(PH_3)_2(C_2H_2)$	NL-SCF	1.256	2.145	110.6	28.7
	NL-SCF+QR	1.268	2.104	105.0	29.5
$Pt(PH_3)_2(C_2H_2)$	NL-SCF	1.252	2.269	105.7	26.1
	NL-SCF+QR	1.280	2.171	99.2	30.2
	Experimental				
C_2H_4[e]		1.339			
$Ni(PPh_3)_2(C_2H_4)$[f]		1.43	1.99	111	
$Ni(PR_2CH_2CH_2PR_2)(C_2Me_4)$[g]		1.42	1.98		26
$Pt(PPh_3)_2(C_2H_4)$[h]		1.434	2.111	112	
C_2H_2[i]		1.207			
$Ni(PPh_3)_2(MeOCH_2CCCH_2OMe)$[j]		1.261	1.897	118	32
$Ni(PPh_3)_2(Me_3SiCCSiMe_3)$[j]		1.256	1.927	112	36.7
$Pd(PPh_3)_2(MeO_2CCCCO_2Me)$[k]		1.279	2.063	107	35
$Pd(PCy_3)_2(F_3CCCCF_3)$[l]		1.271	2.047	110	44
$Pt(PCy_3)_2(F_3CCCCF_3)$[l]		1.260	2.046	110	45
$Pt(PPh_3)_2(PhCCPh)$[m]		1.32	2.04	102	40
$Pd(PPh_3)_2(F_3CCCCF_3)$[j]		1.255	2.028	100	

[a] Bond lengths in angstroms and bond angles in degrees. [b] Reference 8a. [c] Reference 8b. [d] Reference 8c. [e] Reference 32. [f] Reference 33. [g] Reference 34. [h] Reference 35. [i] Reference 36. [j] Reference 37. [k] Reference 38. [l] Reference 39. [m] Reference 40. [n] For C_2H_2, θ is the complement to the CCH angle. For C_2H_4, θ is the angle between the C−C bond and the CH_2 plane.

consider the complexes formed between C_2H_4 or C_2H_2 and the d^{10} fragments $M(PH_3)_2$ with M = Ni,Pd and Pt.

The optimized geometries for $M(PH_3)_2(C_2H_4)$, **3**, and $M(PH_3)_2(C_2H_2)$, **4**, are presented in Table 3 and there compared to *ab initio* results. All DFT calculations were carried out within C_{2v} constraints. The most relevant experimental data[32-40] for similar compounds are also included as reference. A direct comparison between theory and experiment is hampered by the fact that the observed structures have bulky groups on the phosphines and, in some cases, on the olefin and acetylene ligands as well. We shall in the following focus our comparisons on the geometries of the ligated olefins and acetylenes, as well as the impact of relativity on the C−C and M−C distances.

Olefin complexes of the type $M(PR_3)_2$(olefin), **3**, have only been structurally characterized by X-ray crystallography for nickel and platinum. The corresponding palladium complex has been more difficult to study due to the rather labile palladium−olefin bond, and we are not aware of any X-ray structure. The C−C bond of coordinated ethylene is in general elongated considerably compared to the C−C bond in free ethylene with R(C−C) = 1.34 Å. For $Ni(PH_3)_2(C_2H_4)$ and $Pt(PH_3)_2(C_2H_4)$, we calculated the C−C bond lengths as 1.414 and 1.422 Å, respectively, at the NL-SCF+QR level. These values are in good agreement with the experimental estimates of 1.43 and 1.434 Å for $Ni(PPh_3)_2(C_2H_4)$ and $Pt(PPh_3)_2(C_2H_4)$, respectively. Relativity is seen to increase the C−C bond distance by 0.023 and 0.035 Å for respectively palladium and platinum. We note that relativity clearly makes the ethylene double bond in the palladium complex the shortest within the triad. Relativity is also seen to have a strong impact on the M−C bond distances. Thus the Pt−C bond is contracted by 0.10 Å whereas the Pd−C distance is shortened by 0.04 Å. The relativistic contraction

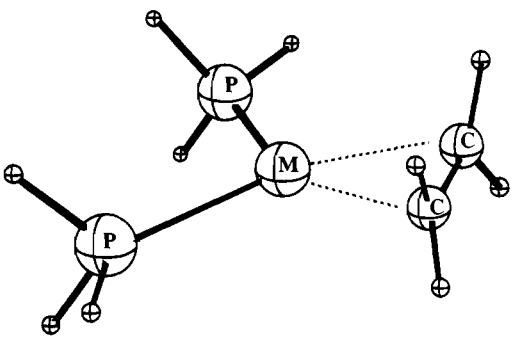

3

(32) Costain, C. C.; Stoicheff, B. P. *J. Chem. Phys.* **1959**, *30*, 777.
(33) Cheng, P. T.; Cook, C. D.; Koo,C. H.; Nyburg,S. C.; Shiomi, M. T. *Acta Crystallogr., B* **1971**, *27*, 1904.
(34) Jolly, P. W.; Wilke, G. *The Organic Chemistry of Nickel;* Academic Press: New York, 1974; Vol. 1.
(35) Cheng, P. T.; Nyburg, S. C. *Can. J. Chem.* **1972**, *50*, 912.
(36) (a) Tanimoto, M.; Kuchitsu, K.; Morino, Y. *Bull. Chem. Soc. Jpn.* **1969**, *42*, 2519. (b) Herzberg, G.; Stoicheff, B. P. *Nature* **1955**, *175*, 79.
(37) (a) Rosenthal, U.; Oehme, G.; Goerls, H.; Burlakov, V. V.; Polyakov, A. V.; Yanovsky, A. I.; Struchkov, Yu. T. *J. Organomet. Chem.* **1990**, *389*, 409. (b) Rosenthal, U.; Oehme, G.; Goerls, H.; Burlakov, V. V.; Polyakov, A. V.; Yanovsky, A. I.; Struchkov, Yu. T. *J. Organomet. Chem.* **1990**, *389*, 251.
(38) McGinnety, J. A. *J. Chem. Soc., Dalton Trans.* **1974**, 1038.
(39) Farrar, D. H.; Payne, N. C. *J. Organomet. Chem.* **1981**, *220*, 251.
(40) Glanville, J. O.; Stewart, J. M.; Grim, S. O. *J. Organomet. Chem.* **1967**, *7*, 9.

results in similar Pt−C and Pd−C bond distances whereas the nonrelativistic order is Pd−C > Pt−C.

For the analogous acetylene complexes, **4**, structures are known for all three members of the triad. Unfortunately, these

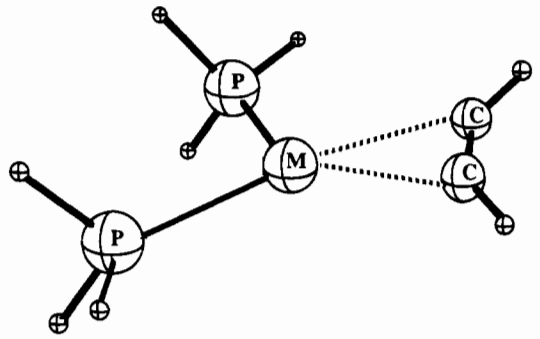

4

structures refer to substituted acetylenes and completely homologous systems with the same substituents are not available for all three metals. However, the experimental C−C distances cover a narrow range from 1.25 to 1.30 Å. The corresponding C−C distance for free acetylene is 1.207 Å. It follows from the DFT calculations that relativity decreases the C−C bonds by 0.028 Å for platinum and 0.012 Å for palladium. In addition, the C−C bond in the palladium complex becomes the shortest after relativity has been included. This is also in line with the experimental observation[41] that the C−C stretching frequencies in a series of homologous acetylene complexes follow the order Pt > Ni > Pd. For the corresponding M−C distances the contractions due to relativity are ΔR(Pt−C) = 0.10 Å and ΔR(Pd−C) = 0.04 Å.

The coordination of C_2H_4 and C_2H_2 to $M(PH_3)_2$ results in angular deformations of the two π-ligands as well as the metal fragment. In ethylene the angle θ_{et} between the C−C bond and the CH_2 planes is increased from the value of 0° in free ethylene. The calculated θ_{et} value of 24° for nickel is in good agreement with the experimental estimate of 26°. The calculated distortions in the palladium and platinum olefin complexes are somewhat smaller, and we note that relativity increases θ_{et} by 4°. With relativity included, the deformation angle θ_{et} follows the order Ni > Pt > Pd. Coodinated accetylene is distorted from the linear conformation by θ_{ac}, which is the complement to the CCH angle. The experimental θ_{ac} values are very dependent on the acetylene substituents but fall in general in the calculated range. We note again a relativistic increase in θ_{ac} by 4° for platinum and a relativistic order for θ_{ac} given by Ni > Pt > Pd. The calculated bending of the PMP angle on the metal fragment is substantial in all the complexes. We find that ∠PMP is largest for palladium. Also, for a given metal, ∠PMP is somewhat (~6°) smaller for **4** compared to **3**. Relativistic effects are seen to reduce ∠PMP for both palladium and platinum and make ∠P−Pd−P the largest within the triad.

There are several structural *ab initio* studies available for comparison, primarily due to Sakaki[8] *et al.* However, these investigations do not cover all three members of a triad and most are carried out at the HF level by varying the geometrical parameters independently. The calculated C−C, M−C, and θ parameters are in general in reasonable agreement with our estimates.

The calculated NL-SCF and NL-SCF+QR bond energies, ΔE, for $(PH_3)_2MC_2H_4$ and $(PH_3)_2MC_2H_2$ are collected in Table 2. In line with those for the dioxygen complexes, the calculated bond energies for **3** and **4** follow the same order Ni ≫ Pt > Pd within the triad, after relativistic effects have been included. This trend is further in agreement with the observed stability order 3d > 5d > 4d, obtained from experimental[31] equilibrium constants for ethylene and acetylene complexes. Relativistic effects are seen to enhance ΔE significantly for Pd and Pt complexes, especially the latter. It is further clear from Table 2 that acetylene forms a slightly stronger bond to a particular metal than ethylene. There are a number of HF calculations on ΔE. Sakaki *et al.* have carried out accurate bond energy calculations for $Ni(PH_3)_2(C_2H_4)$ and $Pt(PH_3)_2(C_2H_4)$ based on post-HF *ab initio* theory and HF geometries. They obtained a value[8b] of 35 kcal/mol for nickel and 20.3 kcal/mol for platinium.

3. Ethylene Complexes $M(CO)_4(C_2H_4)$ (M = Fe, Ru, Os). We have also studied the homologous series of d^8 complexes, **5**, between the $M(CO)_4$ (M = Fe, Ru, Os) fragments and ethylene. The optimized structures for the complexes are given

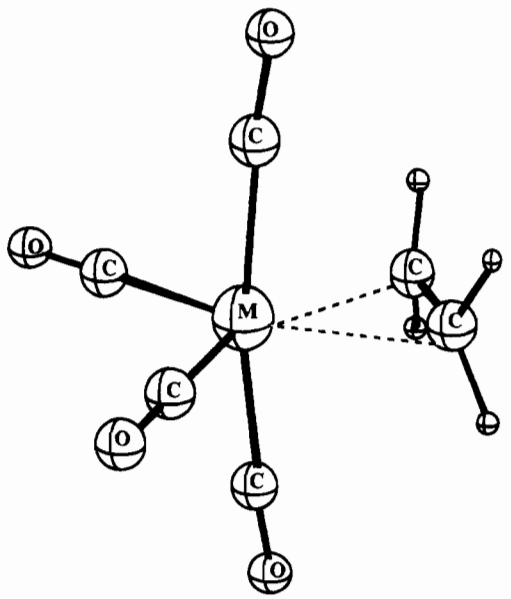

5

in Table 4 together with experimental data[42−46] and results from *ab initio* calculations.[43] The corresponding bond energies are presented in Table 2. The structures for the related $M(CO)_4$ fragments have been published previously.[5b]

We find again that the M−C_2H_4 bond energy is smallest for the 4d element after relativistic effects have been included (NL-SCF+QR), whereas the order is 3d > 4d > 5d in the nonrelativistic limit (NL-SCF), Table 2. Our calculated bond energy for the iron system is given by 39 kcal/mol, in good agreement with an experimental value of 36 ± 4 kcal/mol based on kinetic measurements.[47] The optimized geometry for the iron system is in line with the observed structure, except for the C−C distance, Table 4. However, the C−C bond length carries an experimental uncertainty[47] of ±0.03 Å. For the osmium species our optimized geometry is in good agreement with the *ab initio* structure.[43] On the other hand, the two theoretical structures differ considerably from the experimental geometry.[43] The deviations might in part be due to the large

(41) Greaves, E. O.; Lock, C. J. L.; Maitlis, P. M. *Can. J. Chem.* **1968**, *46*, 3879.
(42) Davis, M. I.; Speed, C. S. *J. Organomet. Chem.* **1970**, *21*, 40.
(43) Bender, B. R.; Norton, J. R.; Miller, M. M.; Anderson, O. P.; Rappe, A. K. *Organometallics* **1992**, *11*, 3427.
(44) Beagley, B.; Schmidling, D. G.; Cruickhark, D. W. *J. Acta Crystallogr., B* **1973**, *29*, 1499.
(45) Takats, J. Private communication.
(46) Ball, R. G.; Burke, M. R.; Takats, J. *Organometallics* **1987**, *6*, 1918.
(47) Brown, D. L. S.; Connor, J. A.; Leung, M. L.; Paz Andrade, M. I.; Skinner, H. A. *J. Organomet. Chem.* **1976**, *110*, 79.

Table 4. Geometries of $M(CO)_4(C_2H_4)^a$

		C−C	M−C	θ	M−C_{ax}	M−C_{eq}	C_aMC_a	C_eMC_e
			Calculated					
$Fe(CO)_4(C_2H_4)$	NL-SCF	1.410	2.130	21.5	1.810	1.820	176.0	112.4
	NL-SCF+QR	1.413	2.128	21.6	1.808	1.818	176.0	112.3
$Ru(CO)_4(C_2H_4)$	NL-SCF	1.416	2.283	20.9	1.987	1.985	176.2	111.6
	NL-SCF+QR	1.422	2.261	21.1	1.962	1.959	176.3	111.3
$Os(CO)_4(C_2H_4)$	NL-SCF	1.418	2.301	23.6	1.992	2.047	170.8	108.4
	NL-SCF+QR	1.428	2.237	24.5	1.992	1.984	170.0	109.0
	HF[b]	1.437	2.249		1.986	1.970	172.0	106.5
			Experimental					
$Fe(CO)_4(C_2H_4)$[c]		1.46	2.117		1.796	1.836		105 ± 2
$Fe(CO)_4(C_2F_4)$[d]		1.53	1.989	41.6	1.823	1.846		104
$Ru(CO)_4(MeO_2CFCCFCOMe_2)$[e]		1.419	2.198		1.959	1.940	179.2	104.5
$Os(CO)_4(C_2H4)$[b]		1.488	2.221		1.943	1.920	171.3	106.0
$Os(CO)_4(Me_3SiCCSiMe_3)$[f]		1.28	2.259		1.93	1.90	172.9	108.6

[a] Bond lengths in angstroms and bond angles in degrees. [b] Reference 43. [c] Reference 42. [d] Reference 44. [e] Reference 45. [f] Reference 46.

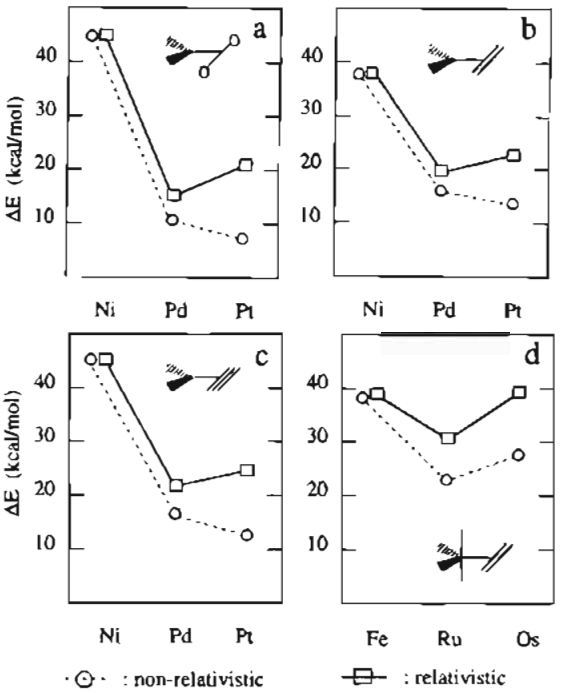

Figure 1. Bond strengths, ΔE's , calculated at the nonrelativistic (dotted line) and the relativistic (solid line) levels.

experimental uncertainties associated with some of the geometrical parameters.

4. Origin of the Relativistic Effects. It follows from the discussion in the previous sections that relativistic effects have an impact on the coordination geometry of the π-ligands (X_2 = O_2, C_2H_2, and C_2H_4) as well as the M−X_2 bond energy. Figure 1 summarizes the bond energy calculations on **2**, **3**, **4** and **5**. The relativistic bond energies display for all systems the characteristic V-shape with a minimum at the 4d element whereas the nonrelativistic bond energies are decreasing through the triad in most cases. The relativistic increase in the M−X_2 bond energy amounts to between 14 and 10 kcal/mol for the 5d elements. A similar V-shaped trend has been observed for metal carbonyl and carbene compounds.[5] The impact of relativity on the M−X and M−P distances is outlined in Figure 2 whereas Figure 3 displays the distortions induced by relativity on the π-ligand X_2. We note again a V-shaped trend in the elongation of the X−X bond as well as the angular distortions, θ_{et} and θ_{ac}, of ethylene and acetylene, Figure 3. We shall now show that the relativistic changes illustrated in Figures 1−3 are related to a relativistic increase in the metal to ligand back-donation, primarily for the 5d elements. We shall, in order to illustrate this point, make use of the extended transition state method[48] (ETS).

The M−X_2 bond energy, ΔE, is written according to the ETS scheme as

$$\Delta E = -(E_{steric} + E_{orb} + E_{prep}) \quad (6)$$

Here E_{steric} represents the steric interaction energy between the metal fragment, ML_n, and X_2. This term is made up of the (stabilizing) electrostatic interaction between X_2 and ML_n as well as the repulsive destabilizing two-orbital−four-electron interactions between occupied orbitals on the two fragments. The repulsive term is usually dominating and E_{steric} as a whole is repulsive. The term E_{orb} originates from stabilizing interactions between occupied and virtual orbitals of the two separate fragments. This term can be divided further into contributions from different symmetry representations (Γ) of the molecular point group according to

$$E_{orb} = \sum_{\Gamma} E_{orb}^{\Gamma} \quad (7)$$

For all the molecules studied here the symmetry group is C_{2v}. Further, the ligand to metal donation, **6a**, takes place in the a_1 representation whereas the metal to ligand back-donation, **6b**, involves the b_2 representation. It is thus possible by the help of eq 7 to separate the contributions to ΔE from the two synergic bonding modes, **6a** and **6b**. The last term, E_{prep}, comes from

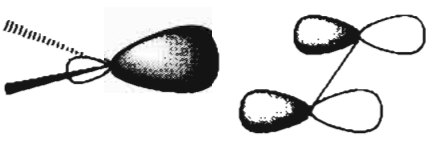

ligand to metal donation

6a

metal to ligand back-donation

6b

(48) (a) Ziegler, T.; Rauk, A. *Theor. Chim. Acta* **1977**, *46*, 1. (b) Ziegler, T. *NATO ASI* **1986**, *C176*, 189. (c) Baerends, E. J.; Rozendaal, A. *NATO ASI* **1986**, *C176*, 159. (d) Ziegler, T. *NATO ASI* **1992**, *C378*, 367.

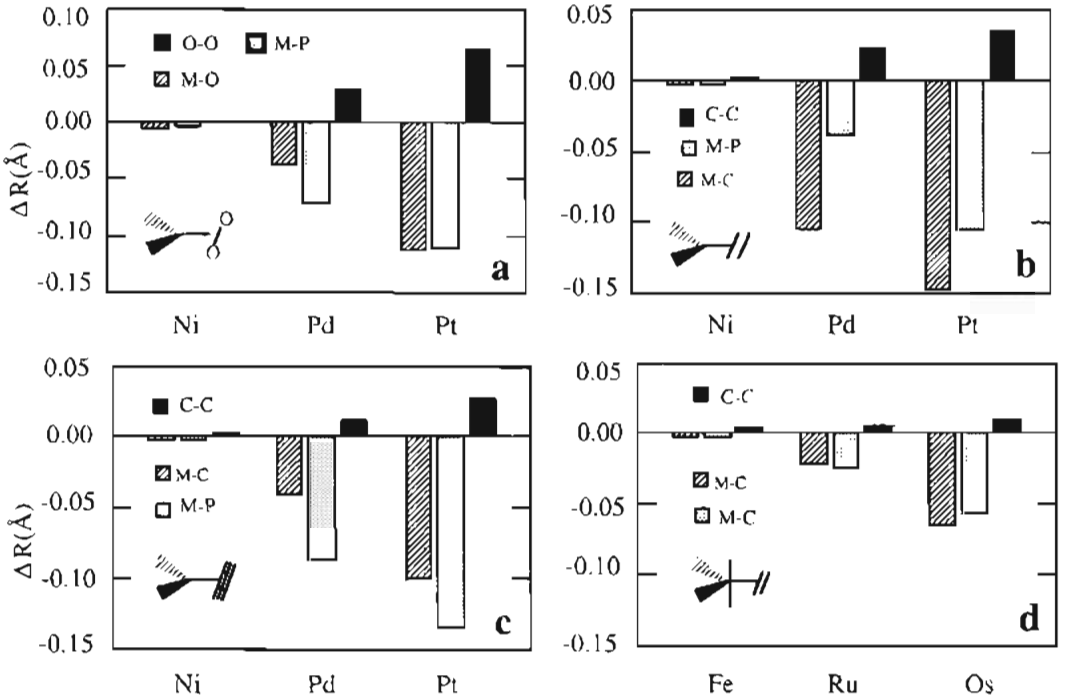

Figure 2. Relativistic effects on M−O, M−C, M−P, O−O and C−C bond lengths.

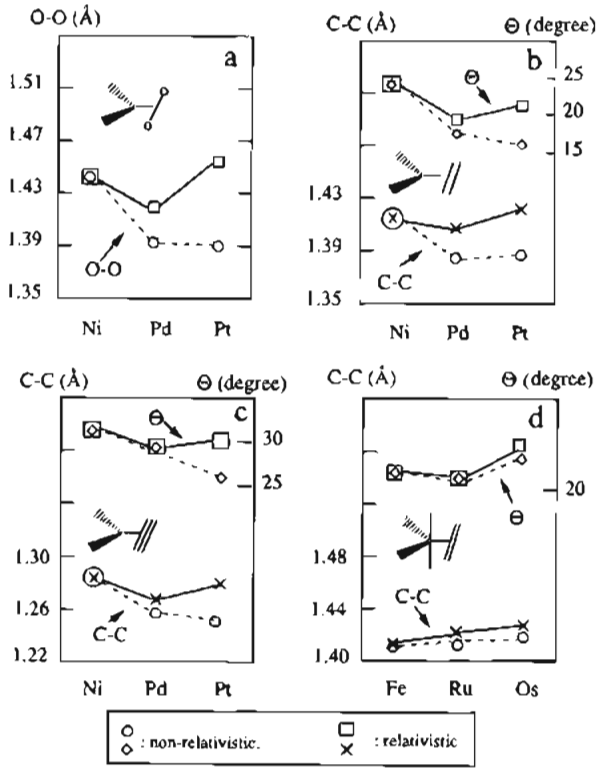

Figure 3. O−O or C−C bond length and back-bending angle, θ, in the ligated species O_2, C_2H_4, or C_2H_2 as calculated at the nonrelativistic (dotted line) and the relativistic (solid line) levels.

the energy required to relax the structures of the free fragments to the geometries they take up in the combined complex. A more detailed description of the ETS scheme and its applications can be found elsewhere.[48] An ETS decomposition of the calculated bond energies for the 5d members of complexes **2**−**5** are given in Table 5 at the nonrelativistic (NR) and relativistic (R) levels of theory, respectively.

It follows from Table 5 that both the donation contribution $-E(a_1)$ from **6a** and the back-bonding contribution $-E(b_2)$ from **6b** are increased by relativistic effects in the d^{10} platinum complexes **2**−**4**. Hence, in the d^{10} complexes relativity is seen to strengthen the $M-X_2$ interaction through both bonding modes. For the d^8 complex $Os(CO)_4(C_2H_4)$, the $-E(a_1)$ donation contribution from **6a** is diminished by relativistic effects while the $-E(b_2)$ back-bonding contribution from **6b** is increased, Table 5. Since the back-donation, $-E(b_2)$, is the dominant part of the bonding interaction, as a whole, the $(CO)_4Os-C_2H_4$ bond is strengthened by relativistic effects, Table 5. For all the systems relativity is seen to decrease the steric repulsion, E_{steric}. This is a direct result of a reduction in the kinetic energy due to the relativistic increase in the electron mass. This effect has been discussed elsewhere.[49]

The relativistic increase in back-donation, **6b**, results in more density flowing into the π* antibonding orbitals of O_2, C_2H_4, and C_2H_2. Therefore, it is quite understandable that relativity induces increases in the O−O and C−C bond lengths and the back-bending angles, θ, of C_2H_4 and C_2H_2, Figure 3.

It now remains to analyze exactly how relativity influences donation and back-donation in the d^{10} and d^8 complexes. Such an explanation can be obtained by looking at the atomic energy levels for the 5d and 6s orbitals in the free atoms, Figure 4. Relativity will in general contract and lower the energy of s-type orbitals.[50] This is a direct effect originating from the fact that s electrons can come close to the nucleus and thus obtain high instantaneous velocities which will result in a reduction of the kinetic energy due to a relativistic mass increase of the electron.[50] The contraction of the s-type orbitals will reduce the effective atomic charge seen by the d electrons and raise their energy. Thus, the d orbitals are destabilized due to an indirect relativistic effect.[50] The atomic energy levels calculated by nonrelativistic and relativistic methods are shown in Figure 4. It can be seen that the 6s atomic orbitals are lowered by 1.29 eV (Pt) and 1.07 eV (Os) whereas the 5d atomic orbitals

(49) (a) Ziegler, T.; Snijders, J. G.; Baerends, E. J. *Chem. Phys. Lett.* **1980**, *75*, 1. (b) Ziegler, T.; Snijders, J. G.; Baerends, E. J.; Ros, P. *J. Chem. Phys.* **1981**, *74*, 1271. (c) Ziegler, T.; Snijders, J. G.; Baerends, E. J. In *The Challenge of d and f Elements, Theory and Computation*; Salahub, D. R., Zerner, M. C., Eds.; ACS Symposium Series 394; American Chemical Society: Washington, DC, 1989.

(50) (a) Pyykkö, P.; Declaux, J.-P. *Acc. Chem. Res* **1979**, *12*, 276. (b) Schwarz,W. H. E.; van Wezenbeek, E. M.; Baerends, E. J.; Snijders, J. G. *J. Phys. B* **1989**, *22*, 1515.

Table 5. Decomposition[c] of ΔE for $Pt(PH_3)_2-O_2$, $-C_2H_4$, or $-C_2H_2$ and $Os(CO)_4(C_2H_4)$ at Nonrelativistic (NR) and Relativistic (R) Levels[a]

		E_{steric}	$-E(a_1)$	$-E(a_2)$	$-E(b_1)$	$-E(b_2)$	$-E_{orb}$[d]	E_{prep}[b]	ΔE[c]
$Pt(PH_3)_2O_2$	NR	110	65	1	3	115	184	69	5
	R	106	71	1	2	124	198	71	21
$Pt(PH_3)_2(C_2H_4)$	NR	41	30	1	3	42	76	23	12
	R	36	32	1	3	48	84	25	23
$Pt(PH_3)_2(C_2H_2)$	NR	51	29	1	4	60	94	33	10
	R	43	40	2	3	67	102	34	25
$Os(CO)_4(C_2H_4)$	NR	55	58	2	3	41	104	25	24
	R	51	33	2	4	79	118	28	39

[a] Energies in kcal/mol. [b] The geometries used in the ETS calculations, in both NR and R cases, are the ones obtained at the NL-SCF+QR level. Therefore, ΔE values for the NR case are slightly different from that in Table 2 due to the E_{prep}. [c] The total bond energy, ΔE, is given according to eq 6 as $\Delta E = -[E_{steric} + E(a_1) + E(a_2) + E(b_1) + E(b_2) + E_{prep}]$. [d] $E_{orb} = E(a_1) + E(a_2) + E(b_1) + E(b_2)$.

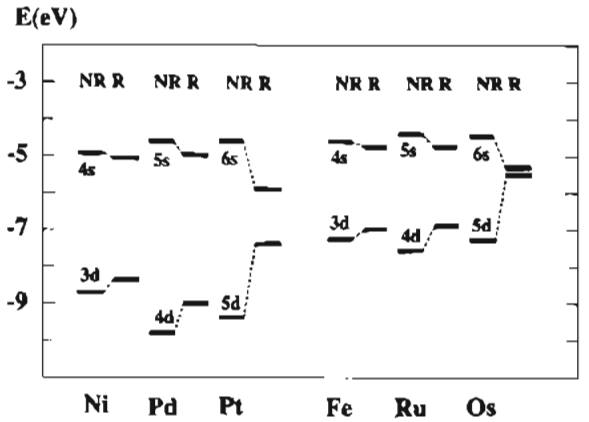

Figure 4. *ns* and $(n-1)$d atomic energy levels of the nickel and iron triads calculated at the nonrelativistic (NR) and relativistic (R) levels. The spin–orbit splittings are averaged out. The spin–orbit splitting will not have an effect in the closed-shell molecules under investigation. The $(n-1)d^{9-1}\ ns^1$ configuration was used in all calculations.

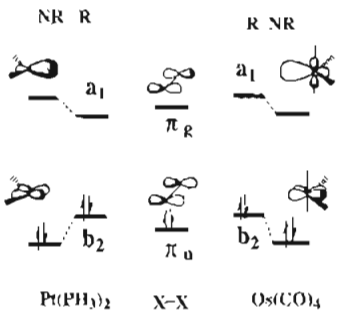

Figure 5. Schematic representation of the influences of relativistic effects on donation and back-donation interactions in M–L bonds.

are raised by 2.02 eV (Pt) and 1.79 eV (Os). We can now apply the trends in the atomic energy levels to the molecular case.

The a_1 acceptor orbital of $Pt(PH_3)_2$ is metal based with a commanding 6s component. The relativistic stabilization of 6s will therefore stabilize this a_1 acceptor orbital of $Pt(PH_3)_2$, diminish the energy gap to the σ-donor orbitals of O_2, C_2H_4 or C_2H_4, and hence enhance the donation interaction, **6a**, as illustrated in Figure 5. At the same time, the relativistic destabilization of the b_2-type d_π donor orbital in $Pt(PH_3)_2$ will close the $d_\pi-\pi^*$ gap of **6b** and enhance back-donation interaction, Figure 5. In $Os(CO)_4(C_2H_4)$, the situation is the same for the back-donation **6b**, Figure 5. However, the donation, **6a**, now involves a metal-based d_σ orbital which is destabilized by relativity. Hence, with a relativistic increase in the $d_\sigma-\sigma$ gap, the donation contribution $-E(a_1)$ is reduced, Figure 5.

Concluding Remarks

Our quasi-relativistic density functional calculations (NL-SCF+QR) revealed that the $M-X_2$ bond strengths for the title compounds display a V-like trend from top to bottom within a triad, with the minimum at the second-row transition metal complexes, Figure 1. Relativity is also responsible for distortions in the coordination geometry of the π-ligand. Again the distortions display a clear V-shaped trend with a minimum at the 4d elements, Figure 3. Relativity is finally seen to influence (contract) the M–C, M–O, and M–P bond distances, Figure 2. Relativistic effects are primarily important for the 5d elements.

The origin of the relativistic effects among the 5d elements is the mass increase for s electrons with high instantaneous velocities near the nucleus. The mass increase will contract and stabilize the s orbitals. This contraction will indirectly increase the energy of the 5d level by reducing the effective nuclear charge experienced by electrons in this level.[50] The destabilization of the d level enhances the metal to ligand back-donation with the result that the $M-X_2$ bond is stabilized further and the X_2 ligand more distorted. We expect that most metal–ligand bonds in which back-donation is the dominating bonding mode will display a V-shaped stability trend within a triad. The V-shape pattern has previously[50] been seen in M_2 and MH systems of the three coinage metals M = Cu, Ag, and Au.

Acknowledgment. This investigation was supported by the Natural Sciences and Engineering Research Council of Canada (NSERC) as well as the donors of the Petroleum Resaerch Fund, administered by the American Chemical Society (ACS-PRF 27023-AC23). J.L. thanks the NSERC for an International Fellowship, and G.S. acknowledges a scholarship from the Department of Chemistry, University of Calgary. We are grateful to Professor J. Takats for the experimental data prior to publication. The Academic Computing Service of the University of Calgary is acknowledged for access to the IBM-6000/RISC facilities.

IC9409118